40 GHz electro-optic modulation in hybrid silicon–organic slotted photonic crystal waveguides

Jan Hendrik Wülbern,[1,*] Stefan Prorok,[1] Jan Hampe,[1] Alexander Petrov,[1] Manfred Eich,[1] Jingdong Luo,[2] Alex K.-Y. Jen,[2] Martin Jenett,[3] and Arne Jacob[3]

[1]*Technische Universität Hamburg-Harburg, E-12, Eissendorfer Straße 38, D-21073 Hamburg, Germany*

[2]*Department of Materials Science and Engineering, University of Washington, Seattle, Washington 98194-2120, USA*

[3]*Technische Universität Hamburg-Harburg, E-3, Denickestraße 22, D-21073 Hamburg, Germany*

**Corresponding author: jan.wuelbern@tu-harburg.de*

Received May 13, 2010; revised July 6, 2010; accepted July 14, 2010;
posted July 21, 2010 (Doc. ID 128451); published August 12, 2010

In this Letter we demonstrate broadband electro-optic modulation with frequencies of up to 40 GHz in slotted photonic crystal waveguides based on silicon-on-insulator substrates covered and infiltrated with a nonlinear optical polymer. Two-dimensional photonic crystal waveguides in silicon enable integrated optical devices with an extremely small geometric footprint on the scale of micrometers. The slotted waveguide design optimizes the overlap of the optical and electric fields in the second-order nonlinear optical medium and, hence, the interaction of the optical and electric waves. © 2010 Optical Society of America

OCIS codes: 130.4110, 130.5296, 160.2100, 160.5293, 190.4710.

Electrically driven optical modulation in silicon photonics typically relies on interactions between the optical mode and the free carrier plasma. [1–3] The achievable modulation speed using these methods is limited by the time constants related to the injection or removal of these free carriers from the optical waveguide. In contrast, electro-optic (EO) modulation via nonlinear optical (NLO) polymers employs the electronic polarization of π-conjugated organic molecules, which allows extremely high modulation speeds extending up to frequencies in the terahertz range. [4] Furthermore, molecular engineering of organic EO materials has led to extremely high Pockels coefficients in polymers, exceeding 300 pm/V [5], which is 10 times the value available in lithium niobate, the standard inorganic material used in EO applications. Photonic devices based on a hybrid material system merging silicon and polymer are therefore attractive, since they combine the strong light-confining abilities of silicon with the superior NLO properties of polymers. EO modulation up to a few megahertz in such hybrid silicon and NLO-polymer systems has been successfully demonstrated for slotted photonic wire-based Mach–Zehnder and ring-resonator modulators [6,7]. Concepts based on slotted photonic crystal (PhC) waveguides can exploit slow-light mechanisms or high-quality-factor cavities to achieve very compact device dimensions and have been discussed [8–10], and modulation with 1.6 Gbit/s has recently been demonstrated [3].

We will use a slotted PhC waveguide in silicon-on-insulator (SOI, $n_{si} = 3.5$), where all void regions are infiltrated with NLO polymer ($n_{Poly} = 1.63$), to demonstrate multigigahertz EO modulation at the transmission edge of the defect mode. The PhC geometry parameters were chosen as follows to allow operation of the device in the C-band telecom regime around 1550 nm: lattice constant $a = 420$ nm, hole radius $r = 0.3a$, waveguide width $W = 1.4a\sqrt{3}$, and slot width $W_{slot} = 150$ nm. The resulting dispersion relation for the TE mode is displayed in Fig. 1, and the inset of the same figure shows a scanning electron micrograph of the structure before the polymer deposition. Slotted waveguides typically show stronger scattering losses than unslotted strip waveguides [7], owing to the field enhancement at the dielectric interface. To keep the propagation through slotted waveguide sections of the whole structure at a minimum, unslotted strip waveguides are used to guide the light to the PhC device. A tapered coupler transition serves to couple the light between the unslotted dielectric access waveguide and the slotted waveguide [11]. The 150-nm-wide slot in the center of the waveguide is filled with NLO polymer. The narrow slot width leads to an optical field enhancement in this region [12]. Consequently, the defect mode frequency is very sensitive to refractive index changes of the NLO polymer, and

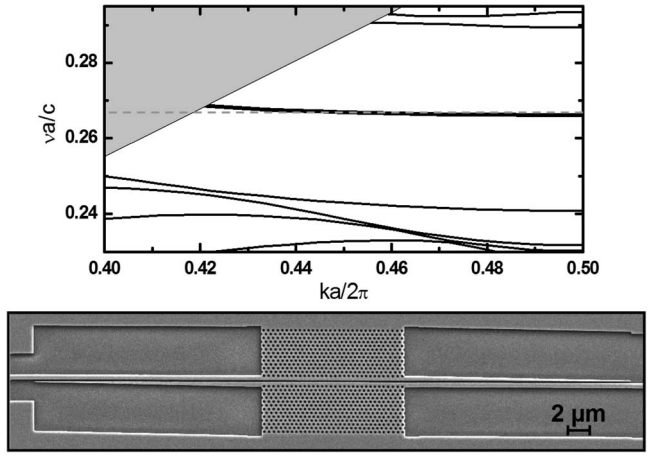

Fig. 1. Top, band diagram of the PhC defect waveguide for TE polarized modes. The thick curve represents the defect mode, the thin curves represent the bulk PhC modes, the dashed curve indicates the position of the optical carrier signal, and the shaded gray region indicates the light cone. Bottom, scanning electron micrograph of the slotted PhC waveguide used for the rf modulation experiments (before the deposition of the NLO polymer). Also shown are the strip-to-slotted waveguide mode converters. The electric field is applied by metal electrodes placed on each side of the structure (not shown here).

the spectral position of the transmission edge can be shifted by an external electric field. Here, this effect will be used to electro-optically modulate the amplitude of a cw input signal tuned closely to the transmission edge of the defect mode.

The devices were fabricated using an etching mask of ZEP-520 electron-beam resist patterned by electron-beam lithography and subsequent inductively coupled plasma etching on a Soitec SOI wafer with a 220-nm-thick Si layer on 2 μm buried oxide. The top layer of silicon was p-doped by ion implantation of boron to a concentration of 10^{18} cm^{-3}, reducing the specific resistance to 0.03 Ωcm. The reduced resistance is necessary to enable a charging time of the slot capacitance of 10 ps, permitting modulation speeds up to 100 GHz, as explained in [10]. A 150 nm gold film was deposited using electron-beam evaporation. The electrical contact pads and rf feeding lines were structured through photolithography and potassium iodide iodine etch. Finally, the samples were covered by a polymer with strong second-order NLO response. The polymer consisted of a guest host system of EO-active chromophore AJ-CKL1 doped 25 wt. % into amorphous polycarbonate (poly[bisphenol-A-carbonate]x-co-[4,4′-(3,3,5-trimethylcyclohexyliddene)diphenol carbonate]) [13]. The polymer was deposited from solution (6 wt. % in cyclopentanone) and subsequently baked at 80 °C under vacuum for 12 h to remove residual solvent.

To align the NLO-chromophores in the slotted region noncentrosymmetrically, the sample was heated to the guest host polymer glass temperature ($T_g = 145$ °C) while applying 20 V poling voltage to the electrodes, resulting in a poling field in the slot of approximately 130 V/μm. After reaching the glass temperature, the sample was rapidly cooled down to room temperature. At room temperature the poling voltage was switched off, thus freezing the molecular orientation of the NLO chromophores in the polymer matrix and preserving the macroscopic EO response in the absence of the poling field.

The transmission properties of the devices were characterized in an end-fire setup using a broadband source (1525–1605 nm bandwidth) and an optical spectrum analyzer. The transmission spectrum of a slotted PhC waveguide device is displayed in Fig. 2; the transmission edge of the defect mode is located near 1533 nm. The low transmission in the passband is predominantly due to the mode mismatch between the slot waveguide mode and the slotted PhC defect mode [10]. Strategies to mitigate these coupling losses are discussed in [10].

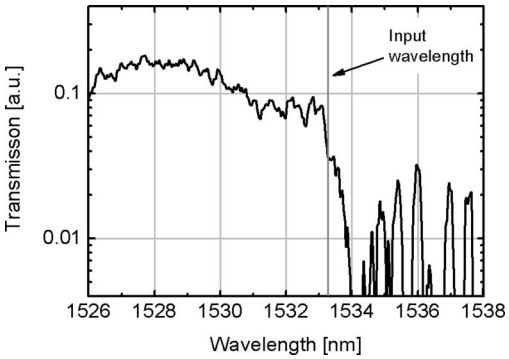

Fig. 2. Transmission spectrum of a 30-lattice-constants long slotted PhC waveguide, infiltrated and covered with NLO polymer. Clearly seen is the transmission edge of the defect mode at 1533 nm. The input wavelength at 1533.2 nm is probing the steep part of the transmission curve.

The response to high frequency modulation was measured using the sideband detection technique. The optical carrier is amplitude modulated with a sinusoidal signal and, hence, the optical spectrum consists of a main peak of the carrier and two side peaks equally spaced around the carrier. The spectral distance from side to main peak is equal to the modulation frequency. In our setup, the carrier was supplied from a tunable narrowband laser source, emitting at 1533.2 nm, close to the transition region from optical passband to stop band, where the slope of the transmission curve is steep. The output signal was detected and spectrally scanned with high resolution around the carrier wavelength using an optical spectrum analyzer.

The resulting optical spectra using modulation frequencies at 15, 20, 30, and 40 GHz are presented in Fig. 3. The sideband frequencies are plotted relative to the carrier, which defines the zero frequency. The sidebands at the correct spectral positions are clearly identifiable at all displayed modulation frequencies. We repeated the experiment in samples where the NLO polymer had not been poled and did not observe any sidebands, proving that the modulation is indeed due to the EO response of the NLO polymer in the slot. At 15 and 20 GHz modulation frequency, the rf power delivered to the chip, including insertion losses from the cable and rf probe, is approximately 13 dBm. From simulations using CST Microwave Studio [14], the modulation voltage at the PhC slot corresponding to this input power is calculated to be 1.4 V_{pp}. From the slope of the transmission spectrum at the carrier frequency, together with the sideband-to-carrier-power ratio, we find the spectral shift to be approximately 40 pm. Both results were confirmed

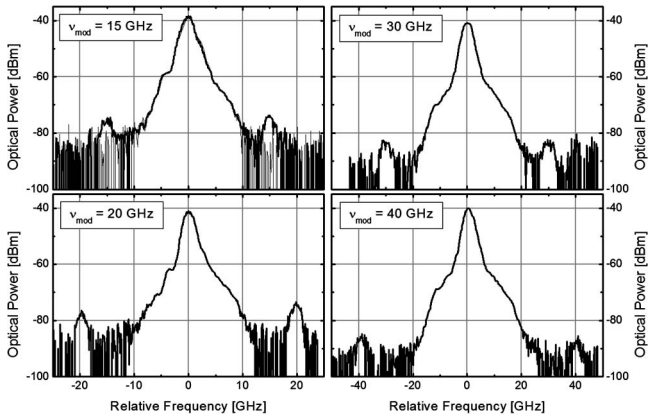

Fig. 3. Optical power spectra of the modulator output at several modulation frequencies measured with an optical spectrum analyzer. The spectral position of the sidebands relative to the optical carrier frequency confirms the EO modulation at microwave frequencies. The gray curve in the upper left plot shows the power spectrum without rf modulation. The 10 dB drop in the sideband power between 15 and 40 GHz is caused by a decrease of the delivered rf power by 6 dB as the frequency is increased from 15 to 40 GHz and a shift in the transmission spectrum due to thermal drift.

by experiments at kilohertz modulation frequencies employing the lock-in measurement technique as explained in [15].

We attribute the drop in sideband power with increasing frequency to the combined effect of reduced output power of the rf source as well as increased insertion loss from the feeding cable and the rf probe, which is estimated to be 6 dB. Additionally, we observed a shift in the transmission spectrum, most likely due to thermal drift, that decreased the slope of the transmission curve at the probing wavelength. The combined effects lead to the observed drop in sideband power of approximately 10 dB.

The calculated in-device Pockels coefficient of the NLO polymer is 12 pm/V, using the technique described in [15]. This value is nearly 1 order of magnitude below the value reported for thin film samples of the same material [13] or other NLO polymers. Thus, the modulation efficiency and, hence, the sideband power bears the potential to be increased by more than 20 dB by increasing the poling efficiency of the slotted device. This phenomenon of reduced poling efficiency has also been recently observed by other research groups [6]. Currently, it is not clear how the silicon oxide surface layer interacts with the host polymer and dipolar chromophore at slot sizes of around 150 nm, or how these interactions possibly influence the achievable poling-induced acentric order. This topic is currently under investigation. The modulation efficiency could be further improved by performing the modulation in a high-quality-factor microcavity resonance or a slow-light slotted PhC waveguide Mach–Zehnder interferometer, as has been proposed in [8,15], respectively.

In conclusion, we demonstrated EO modulation up to 40 GHz in slotted PhC waveguides in SOI covered and infiltrated by NLO polymer. The modulation frequency was limited only by the available rf source and power feeding scheme, and we did not observe any significant roll-off in the modulation signal amplitude up to this value, indicating that operation at even higher bandwidths should be feasible, as the EO effect based on pure electronic displacement polarization is intrinsically ultrafast. The presented device has an extremely small geometric footprint of only about 550 μm^2, with a slotted PhC waveguide spanning only 30 lattice constants in the propagation direction. The EO amplitude modulation was performed at the optical mode transmission edge of the device. We expect to increase the modulation response, e.g., in high-quality-factor resonant structures, and by an improved poling efficiency. These approaches are currently the focus of our research efforts. The presented results show that ultracompact and ultrafast EO modulators can be realized in slotted PhC waveguides based on hybrid silicon and organic materials.

This research was supported by the German Research Foundation (DFG) (EI 391/12-1). The authors acknowledge support from CST, Darmstadt, Germany with their Microwave Studio software, Ralf Steingrüber from the Heinrich-Hertz-Institut Berlin for providing the electron-beam lithography, and Jürgen Bruns from the Technische Universität Berlin for inductively coupled plasma etching.

References

1. L. Liao, A. Liu, J. Basak, H. Nguyen, M. Paniccia, D. Rubin, Y. Chetrit, R. Cohen, and N. Izhaky, Electron. Lett. **43** (2007).
2. Q. Xu, S. Manipatruni, B. Schmidt, J. Shakya, and M. Lipson, Opt. Express **15**, 430 (2007).
3. X. Chen, Y.-S. Chen, Y. Zhao, W. Jiang, and R. T. Chen, Opt. Lett. **34**, 602 (2009).
4. M. Lee, H. E. Katz, C. Erben, D. M. Gill, P. Gopalan, J. D. Heber, and D. J. McGee, Science **298**, 1401 (2002).
5. T.-D. Kim, J. Luo, Y.-J. Cheng, Z. Shi, S. Hau, S.-H. Jang, X.-H. Zhou, Y. Tian, B. Polishak, S. Huang, H. Ma, L. R. Dalton, and A. K.-Y. Jen, J. Phys. Chem. C **112**, 8091 (2008).
6. T. Baehr-Jones, B. Penkov, J. Huang, P. Sullivan, J. Davies, J. Takayesu, J. Luo, T.-D. Kim, L. R. Dalton, A. K.-Y. Jen, M. Hochberg, and A. Scherer, Appl. Phys. Lett. **92**, 163303 (2008).
7. T. Baehr-Jones, M. Hochberg, C. Walker, and A. Scherer, Appl. Phys. Lett. **86**, 081101 (2005).
8. J. M. Brosi, C. Koos, L. C. Andreani, M. Waldow, J. Leuthold, and W. Freude, Opt. Express **16**, 4177 (2008).
9. A. Di Falco, L. O'Faolain, and T. F. Krauss, Appl. Phys. Lett. **92**, 083501 (2008).
10. J. H. Wülbern, A. Petrov, and M. Eich, Opt. Express **17**, 304 (2009).
11. N. N. Feng, R. Sun, L. C. Kimerling, and J. Michel, Opt. Lett. **32**, 1250 (2007).
12. V. R. Almeida, Q. F. Xu, C. A. Barrios, and M. Lipson, Opt. Lett. **29**, 1209 (2004).
13. H. Chen, B. Chen, D. Huang, D. Jin, J. D. Luo, A. K.-Y. Jen, and R. Dinu, Appl. Phys. Lett. **93**, 043507 (2008).
14. Available at www.cst.com.
15. J. H. Wülbern, J. Hampe, A. Petrov, M. Eich, J. Luo, A. K.-Y. Jen, A. Di Falco, T. F. Krauss, and J. Bruns, Appl. Phys. Lett. **94**, 241107 (2009).